Phys Chem Minerals (1985) 12:161–175

PHYSICS AND CHEMISTRY OF MINERALS

The Electronic Structures of Fe^{3+} Coordination Sites in Iron Oxides; Applications to Spectra, Bonding, and Magnetism

David M. Sherman
Dept. of Earth, Atmospheric, and Planetary Sciences, Massachusetts Institute of Technology, Cambridge, MA 02139, USA
Present Address: U.S. Geological Survey, Reston VA 22092, USA

Abstract. The electronic structures of Fe^{3+} coordination sites in hematite and maghemite are obtained from self-consistent field Xα scattered-wave (SCF-Xα-SW) molecular orbital calculations on an octahedral $(FeO_6)^{9-}$ cluster, a trigonally distorted $(FeO_6)^{9-}$ cluster, and a tetrahedral $(FeO_4)^{5-}$ cluster. The electronic structures of these coordination sites should also give a good description of those of Fe^{3+} cations in other oxides and silicates.The overlapping sphere approach to the SCF-Xα-SW formalism is used and is found to give more accurate results than previous calculations on these systems.

Multiplet theory is used to relate the one-electron molecular orbital energies to the ligand field spectra of Fe^{3+} in oxides. Calculated energies of ligand to metal charge transfer transitions agree with experimental data and are used to interpret the near-UV spectra of Fe^{3+} oxides and silicates.

The calculated wavefunctions show that chemical bonds in Fe^{3+} oxides are fairly covalent. Moreover, the Fe–O bond has a strong spin polarization. The spin dependance of the covalency explains how superexchange and the main features of the magnetic structures of iron oxides are predicted from simple $(FeO_6)^{9-}$ and $(FeO_4)^{5-}$ cluster calculations.

Introduction

Oxides and silicates of trivalent iron are major phases in the surface mineralogy of the Earth and Mars. Many aspects of the geochemistry and physics of these minerals, however, are associated with their partially occupied Fe 3*d* orbitals and, as such, can only be understood within the context of quantum chemistry. Several current problems in geochemistry warrant an improved understanding of the electronic structures of iron oxides and silicates. Examples include understanding the mechanisms of photochemical reactions between colloidal iron oxides and organic molecules in natural waters and interpreting the remote-sensed reflectance spectra of the surface mineralogy of Mars.

The electronic wavefunctions of a mineral must be invariant under the symmetry operations defined by its crystal structure. Accordingly, a complete description of the ground state electronic structure of a mineral must be derived using the Bloch wave functions of band theory. On the other hand, the excited states of electrons in transition metal oxides are usually localized and remove the translational symmetry of the crystal. For these "exciton states", Bloch wave functions are inappropriate. Moreover, translational symmetry is completely lost in iron oxides above their Neel or Curie temperatures where they are paramagnetic.

A quite general, and often more realistic, approach to the electronic structure of a solid is the the cluster molecular-orbital method. In this method, the electronic structure of a solid is approximated by that of a finite atomic cluster which represents a basic structural entity of the crystal. The usefulness of this approximation will depend on the spatial extent of atomic interactions in the solid relative to the size of the atomic cluster being used. For the iron oxides, the simplest cluster consists of an iron atom surrounded by its immediate coordination environment. Such a cluster will allow a treatment of the localized electronic states in iron oxides and, hence, could be used to understand electronic spectra, Mössbauer isomer shifts, magnetic hyperfine splittings, and the nature of the Fe–O bond.

The first application of the cluster molecular orbital method to the electronic structure of Fe^{3+} oxides is that of Tossell et al. (1973, 1974). In that study, molecular orbital calculations using the self-consistent field Xα scattered-wave (SCF-Xα-SW) method (described below), were done for an octahedral $(FeO_6)^{9-}$ cluster; the resulting energy levels were used to interpret the electronic spectra (X-ray emission, ESCA and optical) of hematite. SCF-Xα-SW calculations of the electronic structure of a tetrahedral $(FeO_4)^{5-}$ cluster were later done (Tossell 1978) for the interpretation of the electronic spectra of tetrahedrally coordinated Fe^{3+} in magnetite. Other SCF-Xα-SW calculations on $(FeO_4)^{5-}$ clusters were done by Tang Kai et al. (1980) to interpret Mossbauer isomer shifts of Fe^{3+}. Maruthe and Trautwein (1983), using simple extended Huckel calculations on $(FeO_6)^{9-}$ clusters, have interpreted not only isomer shifts but also quadrupule and magnetic hyperfine splittings in the Mössbauer spectra of Fe^{3+} oxides. To data, few accurate calculations have been done which incorporate the distorted geometries found in most Fe^{3+} polyhedra in minerals.

Since the original investigation of Tossell et al. (1973), several improvements to the SCF-Xα-SW method have been developed, among them the use of overlapping atomic spheres rather than the pure "muffin-tin" approximation to the molecular potential. In addition, new experimental

data and theoretical insights on the electronic spectra of iron oxides and other ferric minerals have been obtained.

The purpose of this paper is to present new calculations of the electronic structure of the octahedral $(FeO_6)^{9-}$ and tetrahedral $(FeO_4)^{5-}$ clusters using the improvements in the SCF-Xα-SW method, to extend the $(FeO_6)^{9-}$ cluster calculations to include the trigonally distorted site geometry in hematite, and to place these results in the context of some of the recent spectroscopic investigations of Fe^{3+} oxides and silicates. Regarding the last objective, the relation between the calculated one-electron molecular orbitals and the multiplet state energies investigated spectroscopically will be derived using multiplet theory. It will be shown how the $10Dq$, B and C parameters of ligand field theory relate to the theoretical one-electron orbital energies. Such results can then be used to give insight on how chemical bonds affect the optical spectra of Fe^{3+} minerals. Finally, the calculated molecular orbital wavefunctions will be used to describe the nature of chemical bonding in iron oxides. These results will then be used to relate chemical bonding to the physical properties and crystal chemistry of iron(III) oxides and silicates.

Theory and Method of Calculation

The theory behind the Xα scattered-wave method has been reviewed in a number of works (Johnson and Smith 1972; Johnson 1973; Slater 1974) but will be outlined here for completeness.

The atomic cluster or molecule is partitioned into a set of spheres each of which is centered about a particular atom. Within each of these atomic spheres, the one-electron Schrodinger equation

$$[1/2\nabla^2 + V_c + V_x]\phi_i = \varepsilon_i \phi_i \tag{1}$$

is solved for the orbitals ϕ_i and their energies ε_i. In (1), V_c and V_x are the coulomb and exchange potentials, respectively. These are expressed in terms of the electronic charge density ρ given by

$$\rho = \Sigma(i)\, n_i \phi_i^* \phi_i \tag{2}$$

where n_i is the occupancy of orbital i. From the charge density the coulomb potential is evaluated using electrostatic theory (solving Poisson's equation) while the exchange potential is evaluated using Slater's Xα approximation (Slater 1974)

$$V_x = -6\alpha[3/4\pi\rho]^{1/3} \tag{3}$$

where α is an adjustable scaling factor chosen so that the Xα total energy of the system equals what would be obained using the conventional Hartree-Fock approach (Schwarz 1972). After the individual atomic potentials are calculated to self consistency, they are superimposed to give an initial molecular potential. Within each of the atomic spheres, the new potential is spherically averaged to give a radial potential appropriate for that atomic region. In the interatomic region, the superimposed molecular potential is volume averaged to give a simple constant potential. Finally, a potential for the extra-molecular region is obtained by spherically averaging the potential within the outer sphere. For each region of the cluster, the Schrodinger equation (using the appropriate potential) is solved. The solutions are matched at the sphere boundaries using multiple-scattered wave theory and the result is then used to derive a new molecular potential. The process is repeated iteratively until a self-consistent result is obtained.

Note that the familiar approximation of molecular orbitals as linear combinations of atomic orbitals (LCAO) is not used. The conceptual utility of this approach is retained in the multiple-scattered wave method, however, since the solutions in each region of the cluster are expressed as a summation of functions with definite angular momenta centered at individual atomic sites (partial waves).

Empirically it is found that the wavefunctions and their energies are significantly improved if the atomic spheres are allowed to overlap (Salahub et al. 1976; Norman 1976). This can be understood qualitatively by noting that such overlap will decrease the volume of the interatomic region. In this region, the potential is constant and the wavefunctions are delocalized partial waves. Although this feature simplifies the computation, it is often a poor approximation to the actual physical situation. Any procedure which minimizes the intersphere contribution should improve the resulting wavefunction.

A useful feature of the Xα approximation is that the exchange potential (equation 3) for spin up electrons can be different from that for spin down electrons. This is done simply by setting the charge-density used in the exchange potential to be that due to only electrons with the same spin. This approach is essential for a realistic treatment of open shell systems (e.g., transition metals with unpaired electrons). If unpaired electrons are present, the exchange potentials, and consequently the spin-up (α spin) and spin down (β spin) orbitals and orbital energies, will be different.

In the conventional Hartree-Fock approach, the energy of a spin-orbital ϕ_i, containing n_i electrons, is given by an ionization energy,

$$\varepsilon_i = \langle E(n_i - 1)\rangle = \langle E(n_i)\rangle \tag{4}$$

where $\langle E(n_i)\rangle$ is the total energy of the system when the occupancy of orbital ϕ_i is n_i. This is formally known as Koopman's theorem. Note, however, that its derivation assumes that the orbitals remain unchanged during the ionization; this may often be a poor approximation insofar as one expects the orbitals to "relax" about the new electronic configuration of the ionized state. In the Xα formalism, the orbital eigenvalues have somewhat different meaning: If $\langle E\rangle$ is the total energy of the system, then the orbital eigenvalues ε_i are given by

$$\varepsilon_i = \frac{\partial\langle E(n_i)\rangle}{\partial n_i} \tag{5}$$

Accordingly, the physical nature of the Xα orbital eigenvalues is similar to the notion of "orbital electronegativity".

To evaluate the energy required for a transition between two states one could calculate the total energy of the system in each state and take the difference. Numerically, this would be very inefficient; electronic transition energies are on the order of a few electron volts while total energies are on the order of 10^4–10^5 electron volts. Slater (1974), however, has shown that one may accurately evaluate the difference between the Xα total energies of two states of a system by using the "transition state" concept. The transition state is defined a having orbital occupancies midway between those found in the initial and final states. Given the transition state configuration, it can be shown that the energy difference between the initial and final states of the

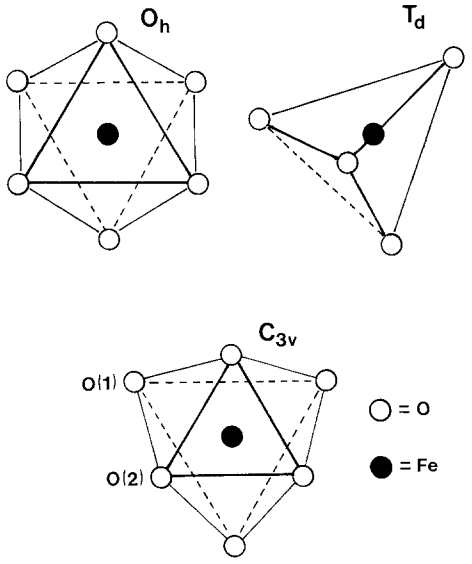

Fig. 1. Geometries of clusters used to model the Fe^{3+} coordination sites in α-Fe_2O_3 and γ-Fe_2O_3 structures

system is given by

$$\Delta E = \langle E \rangle_A - \langle E \rangle_B \simeq \sum_i \{n_A(i) - n_B(i)\}\, \varepsilon_{ts}(i) \quad (6)$$

where $n_A(i)$ and $n_B(i)$ are the occupancies of orbital i in the states A and B, respectively, and $\varepsilon_{ts}(i)$ is the energy of orbital i in the transition state with occupancy

$$n_{ts}(i) = \{n_A(i) + n_B(i)\}/2 \quad (7)$$

One important advantage of the transition state procedure is that it takes into account any orbital relaxation which occurs during the transition.

Cluster Geometries and Input Parameters

The cluster geometries are shown in Figure 1, and the input parameters and bond lengths for each cluster are given in Table 1. The octahedral $(FeO_6)^{9-}$ and tetrahedral $(FeO_4)^{5-}$ clusters are modeled after the coordination sites of Fe^{3+} in maghemite (γ Fe_2O_3) and magnetite (Fe_3O_4). The crystal structure of magnetite is that of an inverse spinel. The structure of maghemite is similar except that vacancies in the tetrahedral A and octahedral B sites give a tetragonal superstructure. The coordination sites in both minerals are of nearly ideal cubic geometry; there is a small trigonal distortion of the octahedral B sites but this was neglected here. Bond lengths were taken from the data of Fasiska (1967).

The third cluster was used to approximate the coordination site of Fe^{3+} in hematite (α Fe_2O_3). This iron oxide has the corundum structure: pairs of face sharing FeO_6 polyhedra occur along the c axis; these dimers, in turn, share edges and corners with each other to form sheets of FeO_6 polyhedra in the plane perpendicular to the c axis. Because of the face-sharing arrangement, the FeO_6 coordination polyhedra have a strong trigonal distortion. One may view each Fe^{3+} center as sandwiched between two triatomic clusters of O^{2-} anions; in the smaller O_3 cluster the oxygen atoms are only 2.67 Å apart whereas in the larger O_3 cluster they are 3.035 Å apart. The two O_3 clusters are slightly

Table 1. Parameters used in cluster calculations

Cluster	Point group	Sphere radii (Å)	Bond lengths (Å)
$(FeO_6)^{9-}$	O_h	Fe =1.186 O =1.245 Out =3.295	Fe–O =2.05 O–O =2.899
$(FeO_4)^{5-}$	T_d	Fe =1.110 O =1.117 Out =2.982	Fe–O =1.865 O–O =3.046
$(FeO_6)^{9-}$	C_{3v}	Fe =1.169 O(1) =1.248 O(2) =1.305 Out =3.342	Fe–O(1) =1.945 Fe–O(2) =2.116 O(1)–O(1) =3.035 O(2)–O(2) =2.669 O(1)–O(2) =2.830

kinked with respect to each other. This lowers the point group symmetry of the FeO_6 polyhedron from C_{3v} to C_3. To simplify the SCF-Xα-SW calculation, this further descent in symmetry was not incorporated into the cluster geometry used here. The Fe–O and O–O bond lengths used for this cluster were determined from the crystal structure data of Blake et al. (1966).

The sphere radii were chosen using the criterion of Norman (1976) and allowing the Fe and O atomic spheres to overlap by about 20%. The resulting virial-theorem ratio T/V (where T and V are the kinetic and potential energies, respectively) is about 2.002 for each cluster. The electrostatic potential of the crystal is approximated by an "inner Watson sphere" (centered about the origin and passing through the oxygen nuclei) and an outer Watson sphere (coincident with the outer sphere). This approach simply allows for different constant potentials to be added to the regions inside and outside of the outer sphere. However, the use of different Watson sphere potentials for the atomic-interatomic and outer sphere regions does not appear to have much effect on the results since most of the orbitals have only a small outer-sphere component.

Partial waves with angular momentum quantum numbers $l=1$ for the oxygen atoms, $l=2$ for the iron atoms, and $l=3$ for the outer spheres were used; that is, for the oxygen atoms only s and p orbitals were included while s, p, and d orbitals were included for the iron atoms. Unlike the LCAO Hartree-Fock methods, the SCF-Xα-SW approach does not have the problems associated with choosing between "minimal" or "extended" basis sets. The "basis set" used here is essentially complete within the context of the approximation.

The α values for the atomic regions are those given by Schwarz (1972) whereas the α values used for the interatomic regions and outer spheres are taken to be the valence-electron weighted average of the atomic values.

Electronic Structure of Octahedral $(FeO_6)^{9-}$

The calculated molecular orbital diagram for the octahedral $(FeO_6)^{9-}$ cluster is shown in its spin-unrestricted form in Figure 2. Each of the orbitals is labelled according to its corresponding irreducible representation of the O_h point group. The energy levels shown are those which fall within the oxygen $2p$ and iron $3d$ bands. These are the orbitals that determine most of the electronic properties of the octa-

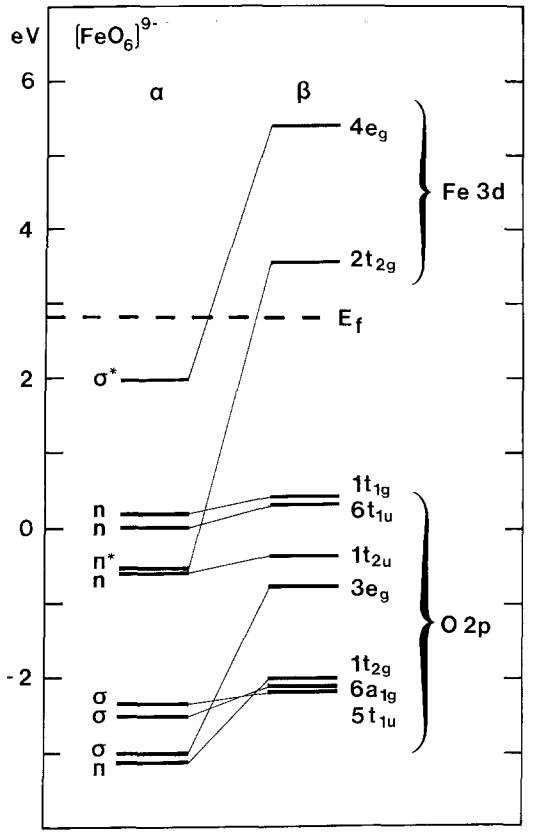

Fig. 2. Molecular orbital diagram of $(FeO_6)^{9-}$ in a spin-unrestricted description. The symbols α and β refer to spin-up and spin-down electron orbitals, respectively. E_f refers to the Fermi-level, below which all orbitals are occupied

hedral Fe^{3+} coordination site. Because of covalency, the orbitals corresponding to the oxygen 2*p* band can have a substantial iron 3*d*, 4*s* or 4*p* component. Likewise, the nominally iron 3*d* orbitals have a significant oxygen 2*p* component. As in other transition metal oxides, however, the metal 3*s*, 3*p* and oxygen 2*s* orbitals are non-bonding. Table 2 gives the composition of the orbitals shown in Figure 2 in terms of the percent intersphere, Fe atomic and O atomic regions. From their atomic compositions, the nature of each orbital can be described.

Oxygen 2p Valence Band Orbitals

Within this set are the orbitals responsible for the Fe–O chemical bond. The $1t_{1g}$, $1t_{2u}$, and, to a lesser extent, $6t_{1u}$ orbitals, however, are non-bonding. The other oxygen 2*p* valence band orbitals set are bonding and result from the overlap of the oxygen 2*p* atomic orbitals with either the iron 3*d*, 4*s* or 4*p* atomic orbitals. The t_{1u} type O 2*p* orbital combinations overlap with the iron 4*p* orbital. The resulting $5t_{1u}$ molecular orbital is quite delocalized, probably because the iron 4*p* atomic orbital has a large radial extent. The a_{1g} type O 2*p* orbital combinations overlap with the Fe 4*s* atomic orbital to give the σ-bonding $3a_{1g}$ orbital. The t_{2g} and e_g type O 2*p* orbital combinations overlap with the Fe 3*d* orbital. The most important bonding orbital is the $2e_g$ which corresponds the Fe(3*d*)–O(2*p*) σ-bonding interaction. Wave function contours for the $2e_g$ orbitals are shown in Figure 3. Of next importance is the $1t_{2g}$ orbital which corresponds the Fe(3*d*)–O(2*p*) π-bonding interaction. This orbital is shown in Figure 4. In contrast to the picture given by most inorganic chemistry texts, there is a large degree of π-bonding in this cluster.

Iron 3d Band Orbitals

The orbitals labelled $2t_{2g}$ and $4e_g$ are the antibonding versions of the $1t_{2g}$ and $2e_g$ bonding molecular orbitals. If the Fe–O bond were purely ionic, the $2t_{2g}$ and $4e_g$ orbitals would be the iron 3*d* atomic orbitals which have lost their degeneracy by electrostatic interaction with the octahedral crystal field. Because of covalency, however, the nominally iron 3*d* orbitals have a significant oxygen 2*p* component. Still, the $2t_{2g}$ and $4e_g$ orbitals are mostly Fe 3*d* in character (Table 2) and localized on the iron atom; because of this, electronic transitions between these orbitals can be treated using ligand field theory. The energy separation between the $2t_{2g}$ and $4e_g$ orbitals in a spin-restricted picture can be equated with the ligand field theory parameter $10Dq$ (Sambe and Felton 1976). Because the $2t_{2g}$ and $4e_g$ orbitals are occupied by only the five α-spin electrons, the α and β-spin versions of each orbital are separated by a large (ca. 4.1 eV) exchange energy. The exchange splittings of these orbitals are directly proportional to Racah *B* and *C* parameters of ligand field theory. Associated with the exchange splitting is the spin polarization of the orbitals;

Table 2. Orbital compositions in the octahedral $(FeO_6)^{9-}$ cluster

	Spin-up orbitals				Spin-down orbitals				
	Energy (eV)	%Fe	%O	%Int.		Energy (eV)	%Fe	%O	%Int.
$7t_{1u}$* (0)	15.74	19	19	52	$7t_{1u}$* (0)	16.36	16	18	54
$7a_{1g}$* (0)	12.83	36	35	26	$7a_{1g}$* (0)	13.89	33	35	29
$4e_g$* (2)	2.01	35	61	4	$4e_g$* (0)	5.44	75	24	1
$1t_{1g}$ (3)	0.20	0	92	8	$2t_{2g}$*(0)	3.58	86	7	6
$6t_{1u}$ (3)	0.01	2	89	8	$1t_{1g}$ (3)	0.44	0	91	8
$2t_{2g}$* (3)	−0.56	48	40	12	$6t_{1u}$ (3)	0.29	2	89	8
$1t_{2u}$ (3)	−0.58	0	86	14	$1t_{2u}$ (3)	−0.36	0	85	14
$5t_{1u}$ (3)	−2.36	3	68	29	$3e_g$ (2)	−0.77	23	73	3
$6a_{1g}$ (1)	−2.50	11	75	14	$1t_{2g}$ (3)	−2.00	7	69	23
$3e_g$ (2)	−2.98	64	35	0	$6a_{1g}$ (1)	−2.09	9	75	15
$1t_{2g}$ (3)	−3.12	49	38	15	$5t_{1u}$ (3)	−2.14	2	68	29

The numbers in parentheses give the orbital occupancies. Orbitals with an asterisk are antibonding

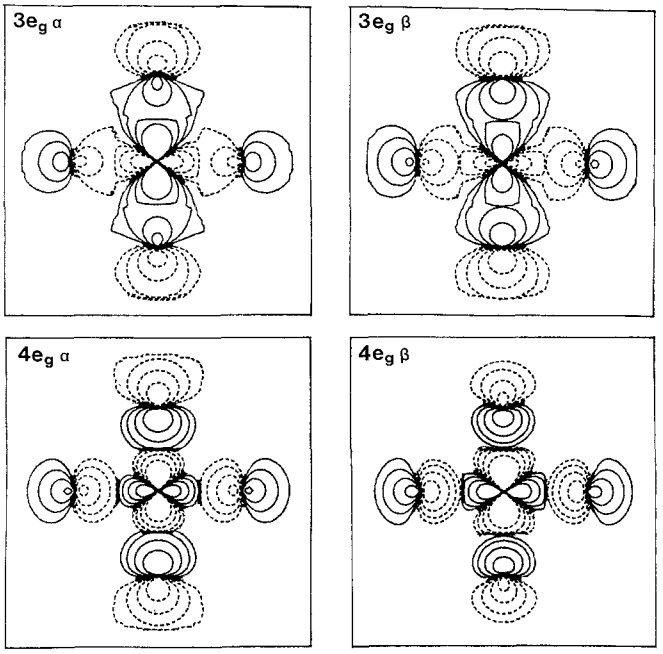

Fig. 3. Wave function contours for the $2e_g$ bonding and $4e_g$ antibonding orbitals of the $(FeO_6)^{9-}$ cluster in the zx or zy plane. The orbitals may be veiwed as consisting of the Fe $3d(z^2)$ atomic orbital and a linear combination of O $2p$ orbitals. Contour intervals are at 0.02, 0.04, 0.08 and 0.16. Solid and dashed contours indicate positive and negative values of the wave function, respectively

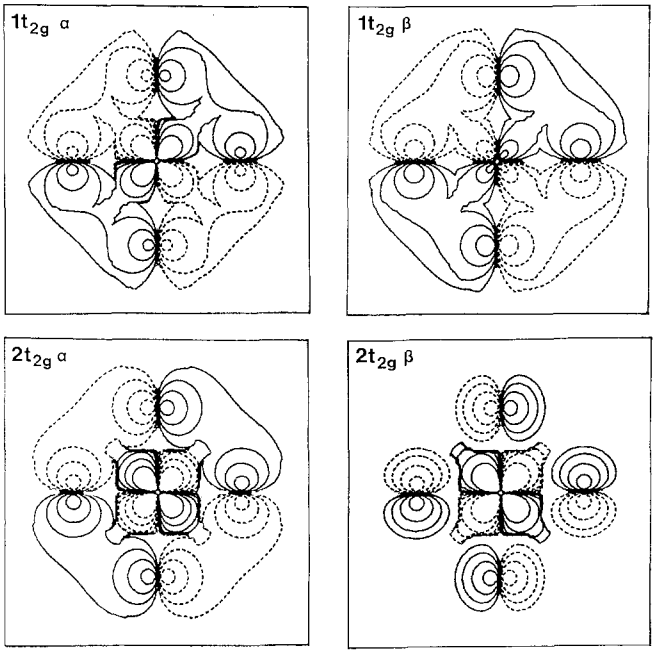

Fig. 4. Wave function contours for the $1t_{2g}$ bonding and $2t_{2g}$ antibonding orbitals in the $(FeO_6)^{9-}$ cluster. These orbitals consist of the Fe $3d(xy)$, $3d(xz)$ or $3d(yz)$ atomic orbitals and a linear combination of O $2p$ orbitals. Contour intervals are as in Figure 3

that is, the spin-up or α-spin orbitals are much less localized than the spin-down or β-spin orbitals. This is shown by the wave function contours for the $2t_{2g}$ and $4e_g$ orbitals given in Figures 3 and 4. Spin-dependence of the electron delocalization has several implications for magnetism and the nature of charge carriers associated with intrinsic semiconduction in iron oxides; these will be discussed in a later section.

Fe 4s, 4p Band Orbitals

The $7t_{1u}$ and $7a_{1g}$ orbitals correspond to the Fe $4p$ and Fe $4s$ atomic orbitals. They are not indicated in Figure 2 but their energies are given in Table 2. Their calculated charge densities, however, show that they are strongly delocalized over the oxygen, intersphere and extramolecular regions. In the molecular orbital description, the $7t_{1u}$ and $7a_{1g}$ orbitals are the antibonding versions of the $5t_{1u}$ and $6a_{1g}$ bonding orbitals.

Electronic Structure of Tetrahedral $(FeO_4)^{5-}$

The spin-unrestricted molecular orbital diagram for the $(FeO_4)^{5-}$ cluster is shown in Figure 5. Again, only the orbitals falling within the oxygen $2p$ and iron $3d$ bands are shown. The compositions of the orbitals shown in Figure 5 are given in Table 3.

Oxygen 2p Valence Band orbitals

The non-bonding oxygen $2p$ orbital combination in the tetrahedral cluster is that of t_1 symmetry. The rest of the

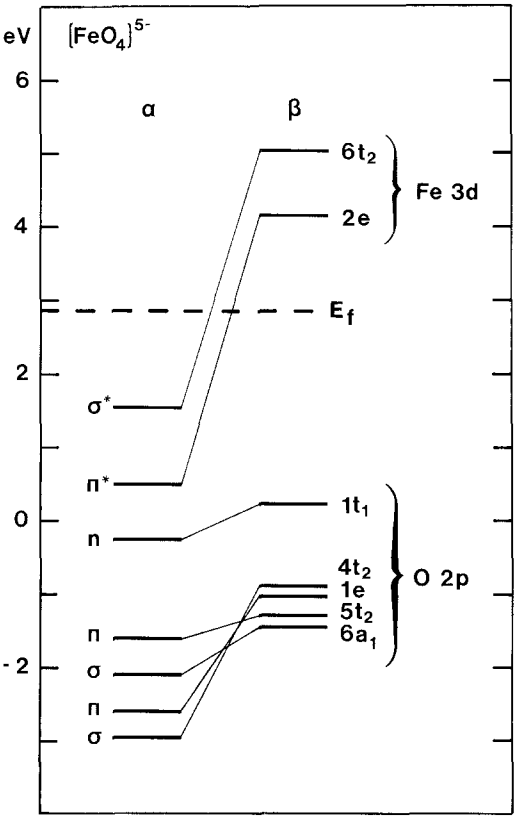

Fig. 5. Molecular orbital diagram for the $(FeO_4)^{5-}$ cluster in a spin-unrestricted description

Table 3. Orbital compositions in the $(FeO_4)^{5-}$ cluster

	Spin-up orbitals				Spin-down orbitals				
	Energy (eV)	%Fe	%O	%Int.		Energy (eV)	%Fe	%O	%Int.
$7a_1$*(0)	14.67	22	21	38	$7a_1$* (0)	15.40	16	18	39
$6t_2$* (3)	1.64	41	50	9	$6t_2$* (0)	5.08	70	20	10
$2e$* (2)	0.53	44	46	10	$2e$* (0)	4.19	81	12	7
$1t_1$ (3)	−0.24	0	85	14	$1t_1$ (3)	0.24	0	86	13
$5t_2$ (3)	−1.65	3	64	33	$4t_2$ (3)	−0.86	21	68	10
$6a_1$ (1)	−2.06	11	71	18	$1e$ (2)	−1.03	11	68	20
$1e$ (2)	−2.57	52	35	13	$5t_2$ (3)	−1.25	3	63	34
$4t_2$ (3)	−2.88	55	40	4	$6a_1$ (1)	−1.43	9	70	21

Numbers in parantheses are the occupancies of the orbitals. For orbitals whose charge distribution does not sum to 100 percent, the remaining charge is located outside the outer sphere

orbitals within the oxygen $2p$ valence band are bonding. The molecular orbitals of t_2 symmetry correspond to both σ- and π-bonding interactions between the oxygen $2p$ orbitals and the iron $3d$ or $4p$ atomic orbitals. In particular, the $4t_2$ orbital corresponds to Fe($3d$)−O($2p$) σ-bonding while the $5t_2$ orbital corresponds to Fe($4p$)−O($2p$) σ- and π-bonding. The $1e$ molecular orbital is the π-bonding interaction between the Fe $3d$ and O $2p$ orbitals. Finally, the $6a_1$ orbital is the O($2p$)−Fe($4s$) σ-bonding interaction.

Iron 3d Band Orbitals

The $2e$ and $6t_2$ orbitals are the antibonding versions of the $1e$ and $4t_2$ bonding molecular orbitals. As with the $2t_{2g}$ and $4e_g$ orbitals of the $(FeO_6)^{9-}$ cluster, the $2e$ and $6t_2$ orbitals of the $(FeO_4)^{5-}$ cluster would be the iron $3d$ orbitals if there were no covalent bonding. The Fe−O bond is only partially covalent and, as such, the $2e$ and $6t_2$ orbitals are mostly iron $3d$ and localized on the iron atom (Table 3). Although allowed by symmetry, there is no Fe($4p$) character in these orbitals.

Iron 4s Band Orbitals

The $7a_1$* orbital is the antibonding version of the $6a_1$ bonding orbital. The former also corresponds to the Fe $4s$ atomic orbital but is found to be strongly delocalized over the oxygen, interatomic, and extra-molecular regions. The energy of this orbital is given in Table 3. At an even higher energy is the $8t_2$ orbital which corresponds to the Fe($4p$) atomic orbital and the antibonding version of the $4t_2$ bonding orbital. The energy of the $6t_2$ orbital was not calculated, however.

The Electronic Structure of Trigonal $(FeO_6)^{9-}$

Figure 6 shows the spin-unrestricted electronic structure of the trigonally distorted $(FeO_6)^{9-}$ cluster used to approximate the coordination polyhedron of Fe^{3+} in hematite and minerals with related structures. Relative to the octahedral $(FeO_6)^{9-}$ cluster discussed previously, the descent in symmetry to C_{3v} splits the triply degenerate orbitals into two-fold-degenerate e and singly degenerate a_1 or a_2 orbitals. The splitting of the orbitals due to the trigonal field in hematite is small, however, and as such, the electronic structures of the octahedral and trigonally distorted clusters are fairly similar.

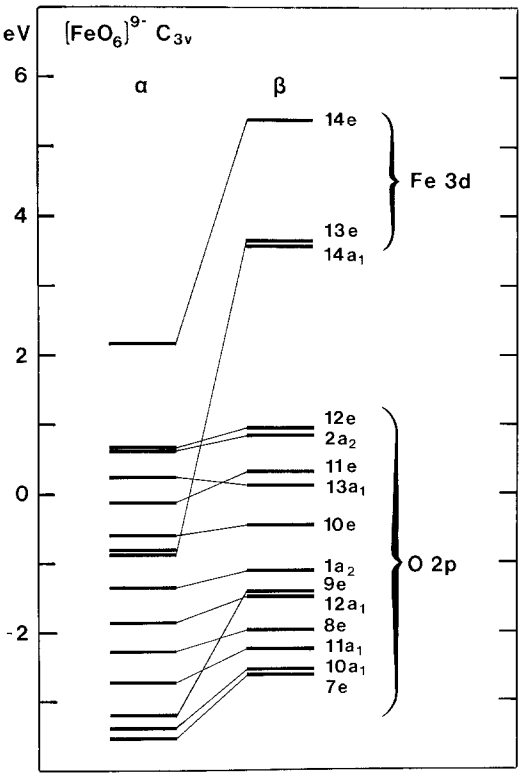

Fig. 6. Molecular orbital diagram for the trigonally-distorted coordination polyhedron in hematite

The orbitals labelled $1a_2$, $10e$, $13a_1$, $11e$, $2a_2$, and $12e$ are all primarily O $2p$ non-bonding orbitals. Formally, the $1a_2$ and $10e$ orbitals result from splitting of the $1t_{1g}$ orbital, the $13a_1$ and $12e$ result from the splitting of the $6t_{1u}$ orbital, and the $10e$ and $1a_2$ result from the splitting of the $1t_{2u}$ orbital. These relations among the orbitals are only a convenience, however, because the the $1t_{2u}$, $6t_{1u}$ and $1t_{1g}$ non-bonding orbitals of the octahedral $(FeO_6)^{9-}$ cluster mix with one another upon going from O_h to C_{3v} symmetry. Hence, for example, the $1a_2$ and $2a_2$ orbitals each result from both the $1t_{1g}$ and $1t_{2u}$ orbitals of the octahedral $(FeO_6)^{9-}$ cluster.

The width of the oxygen $2p$ non-bonding orbital set (about 2 eV) is much greater than that found in the octahedral $(FeO_6)^{9-}$ cluster. This results from the trigonal site distortion. The latter forces the O(2) oxygens to be only 2.67 Å apart which, in turn, increases their repulsive O−O interaction. This raises the energies of the O(2) oxygen $2p$ orbitals and, as such, the highest energy non-bonding orbitals ($9e$, and $2a_2$) are completely localized on the O(2) oxygens. On the other hand, the trigonal site distortion forces the O(1) oxygens to be farther apart with an O(1)−O(1) bond distance of 3.3 Å. This decreases the O(1)−O(1) repulsive interaction and stablizes the O(1) oxygen $2p$ orbitals. Accordingly, the lowest energy oxygen $2p$ non-bonding orbital ($1a_2$) is localized on the O(1) oxygens.

Electronic Spectra of Iron Oxides and Related Minerals

General

The near-infrared, visible and near-ultraviolet spectra of iron (III) oxides and silicates consist of several types of electronic transitions: First, there are the transitions between the different multiplet states arising from the different Fe $3d$ configurations. These states are usually described using ligand field theory where the multiplet state energies are described in terms of the three parameters $10Dq$, B and C. This approach gives the Tanabe-Sugano diagram (Fig. 7) for the states of Fe^{3+}. Second, there are the ligand to metal charge-transfer (LMCT) transitions. These are excitations from the O ($2p$) valence band orbitals (mostly ligand character) to the Fe ($3d$) crystal field type orbitals (mostly metal atom character). These transitions are most easily understood within the context of molecular orbital theory. At much higher energies than the LMCT transitions are the transitions from the Fe $3d$-type orbitals to the Fe $4s$- and $4p$-type orbitals. These will be referred to as metal-to-conduction band (MCB) transitions. Finally, there are transitions which arise from $Fe^{3+}-Fe^{3+}$ pair interactions; these will be discussed in more detail below.

Multiplet Theory for Fe^{3+} Ligand-Field states

The electronic structures of the Fe^{3+} coordination polyhedra are obtained in terms of one-electron orbitals. The actual states of a cluster, atom, or molecule, however, are multielectronic wavefunctions. To use the calculated one-electron orbital energies for the interpretation of the spectra of iron oxides, it is first necessary to show how the one-electron orbitals are related to the actual multielectronic states. This is done using multiplet theory (Slater 1968; 1974) which, because of its importance, will be briefly outlined.

An electronic configuration over one-electron orbitals in general corresponds to several multielectronic states. The latter are referred to as multiplets. The irreducible representations of the multiplets arising from a given electronic configuration are obtained by taking the direct product of the occupied one-electron orbitals. Associated with each multiplet is a spin quantum number S; hence, each multiplet corresponds to $2S+1$ degenerate states with magnetic spin quantum numbers $M_s = S, S-1, \ldots, -S$. Analytically, each M_s state of a multiplet is given by a linear combination of Slater determinents over one-electron orbitals. In order to find the energies to the individual M_s states and, hence, the energies of the multiplets, we must be able to find the energies of the individual Slater determinents arising from a given electronic configuration. In general, this cannot be done.

On the other hand, the energy of an electronic configuration corresponds to the average energy of the Slater determinants that are consistent with that configuration. This, in turn corresponds to the average energy of the M_s states of the multiplets that are constructed from those Slater determinants. It should also be noted that a spin-unrestricted calculation allows us to set up a configuration with a given value of the magnetic spin quantum number M_s. This gives us much more information since the energy of such a configuration corresponds to the average energy of only the Slater determinents resulting from that configuration which have that value of M_s. This energy, in turn, corresponds to the average energy of the multiplets with components that can be constructed with these Slater determinents (that is, the multiplets whose spin quantum number S is greater than or equal to M_s). In other words, the energy of a configuration with a given M_s corresponds to the average energy of the multiplets arising from that configuration that have $S \geqq M_s$.

The following discussion will be based on Fe^{3+} in octahedral coordination; the results for Fe^{3+} in tetrahedral coordination follow directly. The ground-state electronic configuration of octahedrally coordinated Fe^{3+} is $(2t_{2g})^3(4e_g)^2$. This configuration corresponds to 120 Slater determinants and, hence, 120 states. The individual states group to give the multiplets:

$$3(^2A_2)+3(^2E)+4(^2T_1)+4(^2T_2)+2(^4E)+{}^4T_1+{}^4T_2+{}^4A_1+{}^4A_2+{}^6A_1$$

The energy of the $(2t_{2g})^3(4e_g)^2$ configuration corresponds to the average energy of these multiplets. However, we are only interested in the quartet and hextet multiplets since those are the only ones observed experimentally. The average energies of the doublet, quartet and hextet multiplets can be found from the energies of the $(2t_{2g})^3(4e_g)^2$ type configurations in a spin-unrestricted calculation.

First, we wish to find the energy of the ground $^6A_1$ multiplet. The $M_s = 5/2$ component of this multiplet is the only state which arises from the $t_{2g}{}^3e_g{}^2$ configuration with $M_s = 5/2$ (that is, the spin unrestricted configuration $(2t_{2g}{}^{\alpha})^3(4e_g{}^{\alpha})^2$). Hence, the energy of the $^6A_1$ multiplet is equal to the energy of the $(2t_{2g}{}^{\alpha})^3(4e_g{}^{\alpha})^2$ configuration.

Next, we wish to find the energies of the quartet multiplets arising from the $t_{2g}{}^3e_g{}^2$ configuration. The $M_s = 3/2$ components of these multiplets, together with the $M_s = 3/2$ component of the $^6A_1$ multiplet, arise from the $t_{2g}{}^3e_g{}^2$ configurations that have $M_s = 3/2$—namely, the $(2t_{2g}{}^{\alpha})^2(4e_g{}^{\alpha})^2(2t_{2g}{}^{\beta})^1$ and $(2t_{2g}{}^{\alpha})^3(4e_g{}^{\alpha})^1(4e_g{}^{\beta})^1$ spin-unrestricted configurations. There are thirteen Slater determinants with $M_s = 3/2$ arising from the $t_{2g}{}^3e_g{}^2$ configuration. The energy of the $(2t_{2g}{}^{\alpha})^2(4e_g{}^{\alpha})^2(2t_{2g}{}^{\beta})^1$ configuration corresponds to the average energy of nine of these determinents while the energy of the $(2t_{2g}{}^{\alpha})^3(4e_g{}^{\alpha})^1(4e_g{}^{\beta})^1$ configuration corresponds to the average energy of the remaining four determinants. Hence, the average energy of all the $M_s = 3/2$ determinantal wavefunctions associated with the $(2t_{2g})^3(4e_g)^2$ configuration is given by

$$\langle E(M_s = 3/2)\rangle = (1/13)(9\langle E_1\rangle + 4\langle E_2\rangle) \quad (8)$$

Table 4. Calculated optical spectra of Fe^{3+} oxides

One-electron transition	Energy (kK)*	Corresponding spectroscopic transitions	Comments
$(FeO_6)^{9-}$ O_h			
$6t_{1u}^{\beta} \rightarrow 4e_g^{\beta}$	51.9	$6A_{1g} \rightarrow {}^6T_{1u}, {}^6T_{2u}$	LMCT
$1t_{2u}^{\beta} \rightarrow 2t_{2g}^{\beta}$	43.6	${}^6A_{1g} \rightarrow {}^6A_{1u}, {}^6E_u, {}^6T_{1u}, {}^6T_{2u}$	LMCT
$6t_{1u}^{\beta} \rightarrow 2t_{2g}^{\beta}$	38.1	${}^6A_{1g} \rightarrow {}^6A_{2u}, {}^6E_u, {}^6T_{1u}, {}^6T_{2u}$	LMCT
$2t_{2g}^{\alpha} \rightarrow 2t_{2g}^{\beta}$	29.3	${}^6A_{1g} \rightarrow {}^4E_g, {}^4A_{1g}({}^4G), {}^4T_{2g}({}^4D),$	
$4e_g^{\alpha} \rightarrow 4e_g^{\beta}$	25.4	${}^4E_g({}^4D), {}^4T_{1g}({}^4P), {}^4A_{2g}({}^4F)$	Ligand field
$4e_g^{\alpha} \rightarrow 2t_{2g}^{\beta}$	11.1	${}^6A_{1g} \rightarrow {}^4T_{1g}({}^4G), {}^4T_{2g}({}^4G)$	Ligand field
$(FeO_4)^{5-}$			
$1t_1^{\beta} \rightarrow 2e^{\beta}$	40.4	${}^6A_1 \rightarrow {}^6T_1, {}^6T_2$	LMCT
$2e^{\alpha} \rightarrow 2e^{\beta}$	26.0	${}^6A_1 \rightarrow {}^4E, {}^4A_1({}^4G), {}^4T_2({}^4D),$	
$6t_2^{\alpha} \rightarrow 6t_2^{\beta}$	23.0	${}^4E({}^4D), {}^4T_1({}^4P), {}^4A_2({}^4F)$	Ligand field
$6t_2^{\alpha} \rightarrow 2e^{\beta}$	16.2	${}^6A_1 \rightarrow {}^4T_1({}^4G), {}^4T_2({}^4G)$	Ligand field

* 1 kK = 1000 cm^{-1} = 0.124 eV

where $\langle E_1 \rangle$ and $\langle E_2 \rangle$ are the energies of the $(2t_{2g}^{\alpha})^2(4e_g^{\alpha})^2(2t_{2g}^{\beta})^1$ and $(2t_{2g}^{\alpha})^3(4e_g^{\alpha})^1(4e_g^{\beta})^1$ configurations, respectively. By the diagonal sum rule, $\langle E(M_s=3/2) \rangle$ also corresponds to the average energy of all multiplets associated with the $(2t_{2g})^3(4e_g)^2$ configuration which have an $M_s=3/2$ component. These are the ${}^6A_1$ and the quartet multiplets given above. Now we are able to calculate the average energy difference between the quartet states that arise from the $(2t_{2g})^3(4e_g)^2$ configuration and the ground ${}^6A_{1g}$ state: From equation (8), the total energy of all the $M_s=3/2$ determinental wavefunctions is $9\langle E_1 \rangle + 4\langle E_2 \rangle$. This corresponds to the total energy of all the multiplets which have an $M_s=3/2$ component. Of these, there are 12 quartet and 1 hextet multiplets. Hence,

$$12\langle E(S=3/2) + \langle E(S=5/2) \rangle = 9\langle E_1 \rangle + 4\langle E_2 \rangle \tag{9}$$

Rearranging gives,

$$\begin{aligned}\langle E(S=3/2) \rangle - \langle E(S=5/2) \rangle &= (3/4)\{\langle E_1 \rangle - \langle E(S=5/2) \rangle\} \\ &+ (1/3)\{\langle E_2 \rangle - \langle E(S=5/2) \rangle\}\end{aligned} \tag{10}$$

The quantities $\{\langle E_1 \rangle - \langle E(S=5/2) \rangle\}$ and $\{\langle E_2 \rangle - \langle E(S=5/2) \rangle\}$ can be readily evaluated using the transition state procedure: $\{\langle E_1 \rangle - \langle E(S=5/2) \rangle\}$ and $\{\langle E_2 \rangle - \langle E(S=5/2) \rangle\}$ correspond to the energies of the $2t_{2g}^{\alpha} \rightarrow 2t_{2g}^{\beta}$ and $4e_g^{\alpha} \rightarrow 4e_g^{\beta}$ one-electron orbital transitions. From the $(FeO_6)^{9-}$ cluster calculation, the $2t_{2g}^{\alpha} \rightarrow 2t_{2g}^{\beta}$ and $4e_g^{\alpha} \rightarrow 4e_g^{\beta}$ one-electron orbital transitions are calculated to have energies of 29.3 and 25.4 kK, respectively (Table 4). Hence, the average energy of the ${}^4E$, ${}^4A_1({}^4G)$, ${}^4T_2({}^4D)$, ${}^4E({}^4D)$, ${}^4T_1({}^4P)$ and ${}^4A_2({}^4F)$ multiplets, relative to the ${}^6A_1({}^4G)$ multiplet, is 30.4 kK. For the $(FeO_4)^{5-}$ cluster, the theoretical barycenter energy of the quartet multiplets arising from the $(e)^2(t_2)^3$ configuration is 25.9 kK.

Finally, we consider the multiplets arising from the excited-state one-electron orbital configuration $t_{2g}{}^4e_g{}^1$ of $(FeO_6)^{9-}$. We are interested only in the quartet multiplets that result from this configuration (that is, the ${}^4T_{1g}({}^4G)$ and ${}^4T_{2g}({}^4G)$ multiplets), since these are the only ones observed experimentally. Hence, we are only interested in the $M_s=3/2$ $t_{2g}{}^4e_g{}^1$ configuration, $(2t_{2g}^{\alpha})^3(4e_g^{\alpha})^1(2t_{2g}^{\beta})^1$. The energy of this configuration is the average energy of the ${}^4T_{1g}({}^4G)$ and ${}^4T_{2g}({}^4G)$ multiplets. Hence, the average energy of the ${}^6A_{1g} \rightarrow {}^4T_{1g}$ and ${}^6A_{1g} \rightarrow {}^4T_{2g}$ spectroscopic transitions is given by the difference between the $2t_{2g}{}^{\beta}$ and $4e_g{}^{\alpha}$ orbital energies in the transition state configuration $(2t_{2g}^{\alpha})^3(4e_g^{\alpha})^{1.5}(2t_{2g}^{\beta})^{0.5}$. This is calculated to be 11.13 kK. From the $(FeO_4)^{5-}$ cluster orbital energies, the average energy of the ${}^6A_1 \rightarrow {}^4T_1$ and ${}^6A_1 \rightarrow {}^6A_1 \rightarrow {}^4T_2$ transitions of tetrahedrally coordinated Fe^{3+} is calculated to be 16.2 kK.

Estimation of Ligand Field Theory Parameters

The meaning of the ligand field theory parameter $10Dq$ in the context of one-electron molecular orbital theory has been uncertain. Sambe and Felton (1976) have shown, using the hyper-Hartree-Fock energy functional (Slater 1974) that $10Dq$ does have meaning in the context of spin-restricted $X\alpha$ one-electron molecular orbitals. For the case of the $(FeO_6)^{9-}$ cluster, $10Dq$ is the $4e_g - 2t_{2g}$ one-electron orbital energy difference in the spin-restricted configuration $t_{2g}{}^3e_g{}^2$. Similarly, for the $(FeO_4)^{5-}$ cluster, $10Dq$ is the $5t_2 - 2e$ one-electron orbital energy difference in the configuration $(2e)^2(5t_2)^3$. (The relation is not as straightforward for other transtion metal ions.) From the spin-restricted calculation of the octahedral $(FeO_6)^{9-}$ cluster, the parameter $10Dq$ is calculated to be 15.8 kK. In the trigonally-distorted $(FeO_6)^{9-}$ cluster, $10Dq$ decreases slightly to 15.0 kK. For the tetrahedral $(FeO_4)^{5-}$ cluster, $10Dq$ is calculated to be 8.23 kK. The ligand field theory expression for the average energy of the ${}^4T_1({}^4G)$ and ${}^4T_1({}^4G)$ states that arise from the $(t_{2g})^3(e_g)^1$ configuration of $(FeO_6)^{9-}$ or the $(t_2)^2(e)^3$ configuration of $(FeO_4)^{5-}$ is (Lever 1968)

$$E = -10Dq + 14B + 6C \tag{11}$$

(Note that this expression neglects the configuration interaction terms.) This energy was calculated from the one-electron orbital energies to be 11.1 kK in the $(FeO_6)^{9-}$ cluster and 16.2 kK in the $(FeO_4)^{5-}$ cluster. The ligand field theory expression for the approximate average energy of the quartet states arising from the $(t_{2g})^3(e_g)^2$ configuration of $(FeO_6)^{9-}$ (or the $(e)^2(t_2)^3$ configuration of $(FeO_4)^{5-}$) can be derived from the Tanabe-Sugano expressions for the energies of these states (e.g. Lever 1968). This gives

$$E = (91/6)B + (17/3)C \tag{12}$$

This was calculated to be 30.4 kK for the $(FeO_6)^{9-}$ cluster and 25.9 kK in the $(FeO_4)^{5-}$ cluster. Given equations (11) and (12), and the previously calculated values for $10Dq$,

we might be able to calculate values for the Racah B and C parameters. Unfortunately, the small (20%) relative errors in the theoretical average state energies give very large relative errors in the Racah B and C parameters values. If, instead, we assume that $C=4.7B$ as in the free-ion, then for the $(FeO_6)^{9-}$ cluster we get $B=727\ cm^{-1}$ from the $(t_{2g})^4(e_g)^1$ configuration (Eq. 11) and $B=637\ cm^{-1}$ from the $(t_{2g})^3(e_g)^2$ configuration (Eq. 12). Similarly, for the $(FeO_4)^{5-}$ cluster, we get $B=579\ cm^{-1}$ from the $(t_2)^4(e)^1$ configuration and $B=620\ cm^{-1}$ from the $(t_2)^3(e)^2$ configuration.

Ligand to Metal Charge-Transfer Transitions

In the $(FeO_6)^{9-}$ cluster, the lowest energy allowed one-electron LMCT transitions are $6t_{1u}^{\beta}\rightarrow 2t_{2g}^{\beta}$ and $6t_{1u}^{\beta}\rightarrow 4e_g^{\beta}$. The one-electron $6t_{1u}^{\beta}\rightarrow 2t_{2g}^{\beta}$ transition corresponds to a set of spectroscopic transitions $^6A_{1g}\rightarrow {}^6T_{1u}$, $^6A_{2u}$, ^6E_u, $^6T_{2u}$. Of these, only the $^6A_{1g}\rightarrow {}^6T_{1u}$ transition is allowed by the Laporte (or parity) selection rule. The $6t_{1u}^{\beta}\rightarrow 4e_g^{\beta}$ transition corresponds to two spectroscopic transitions $^6A_{1g}\rightarrow {}^6T_{1u}$, $^6T_{2u}$ and, again, only the $^6A_{1g}\rightarrow {}^6T_{1u}$ is allowed.

The energies of the LMCT excited states arising from a given one-electron orbital LMCT transition should be very similar. Consequently, for example, the energy of the $6t_{1u}^{\beta}\rightarrow 2t_{2g}^{\beta}$ one-electron orbital transition should be approximately equal to the energy of the observed $^6A_{1g}\rightarrow {}^6T_{1u}$ transition that results from the $6t_{1u}^{\beta}\rightarrow 2t_{2g}^{\beta}$ one-electron orbital transition. This can be argued using an approach similar to that of Verdonck and Vanquickenborne (1976). Consider the transition $6t_{1u}^{\beta}\rightarrow 2t_{2g}^{\beta}$ in $(FeO_6)^{9-}$. The excited-state electronic configuration is $(6t_{1u}^{\alpha})^3(6t_{1u}^{\beta})^2(2t_{2g}^{\alpha})^3(2t_{2g}^{\beta})^1(4e_g^{\alpha})^2$. This may be thought of as consisting of a $(6t_{1u}^{\alpha})^3(6t_{1u}^{\beta})^2$ sub-configuration over the ligand non-bonding orbitals and a $(2t_{2g}^{\alpha})^3(2t_{2g}^{\beta})^1(4e_g^{\alpha})^2$ subconfiguration over the Fe(3*d*)-type antibonding orbitals. Now the $(6t_{1u}^{\alpha})^3(6t_{1u}^{\beta})^2$ subconfiguration yields the term $^1T_{1u}$. Likewise, the $(2t_{2g}^{\alpha})^3(2t_{2g}^{\beta})^1(4e_g^{\alpha})^2$ subconfiguration yields the term $^5T_{2g}$. The $^6T_{1u}$, $^6A_{2u}$, ^6E_u, $^6T_{2u}$ excited states arising from the $6t_{1u}^{\beta}\rightarrow 2t_{2g}^{\beta}$ one-electron transition, therefore, result from the direct product of the $^1T_{1u}$ and $^5T_{2g}$ terms arising from the two subconfigurations. This implies that the spread in energy of the different LMCT excited states ($^6T_{1u}$, $^6A_{2u}$, ^6E_u, $^6T_{2u}$) arising from the $6t_{1u}^{\beta}\rightarrow 2t_{2g}^{\beta}$ transition is dependent only on the interelectronic repulsion between the Fe 3*d* ($2t_{2g}$) and O 2*p* ($6t_{1u}$) orbital electrons. Intuitively, we expect this repulsion to be small since the ligand-type non-bonding orbitals and the Fe 3*d*-type antibonding orbitals have very different spatial distributions. Accordingly, the different states arising from the $6t_{1u}^{\beta}\rightarrow 2t_{2g}^{\beta}$ transition should have similar energies. (The same argument can be made for the $6t_{1u}^{\beta}\rightarrow 4e_g^{\beta}$ transition.) This being the case, it should be a good approximation to equate an observed LMCT transition to a one-electron orbital transition. This approximation will probably fail, however, when one is considering transitions from the bonding O 2*p* valence band orbitals to the Fe 3*d* band orbitals. This is because of the repulsion between the bonding orbital electrons and Fe 3*d* band orbital electrons.

It is of interest to consider the effect of trigonal site distortions on the LMCT energies of the $(FeO_6)^{9-}$ clusters. Tossell (1980) calculated the electronic structure of a $(FeO_6)^{9-}$ cluster with C_{2v} symmetry (one O–O distance shortened) and found that the energy separation between the Fe 3*d* and O 2*p* bands was decreased from that found in an octahedral $(FeO_6)^{9-}$ cluster. It was suggested that, in accordance with the smaller energy gap, the LMCT transition energies will also be smaller. This would have some important geophysical consequences and, as such, warrents discussion. In the $(FeO_6)^{9-}$ cluster with C_{3v} symmetry investigated here, we also find a significant decrease in the energy separation between the O 2*p* and Fe 3*d* bands. This does not imply, however, that the LMCT transition energies will be smaller. To understand why this is the case, it is worthwhile to digress on the nature of the LMCT excited states in O_h and C_{3v} symmetry.

In O_h symmetry, the $6t_{1u}\rightarrow 2t_{2g}$ transition corresponds to a set of spectroscopic transitions

$$^6A_{1g}\rightarrow {}^6A_{2u},\ {}^6E_u,\ {}^6T_{1u},\ {}^6T_{2u} \tag{13}$$

Upon descent to C_{3v} symmetry, the different states in (13) are split to give

$$^6A_1\rightarrow {}^6A_2,\ {}^6E,\ {}^6A_1,\ {}^6E,\ {}^6A_2,\ {}^6E \tag{14}$$

Similarly the $1t_{2u}\rightarrow 2t_{2g}$ one-electron transition in octahedral symmetry corresponds to a set of spectroscopic transitions

$$^6A_{1g}\rightarrow {}^6A_{1u},\ {}^6E_u,\ {}^6T_{1u},\ {}^6T_{2u} \tag{15}$$

which split in C_{3v} symmetry to give

$$^6A_1\rightarrow {}^6A_1,\ {}^6E,\ {}^6A_1,\ {}^6E,\ {}^6A_2,\ {}^6E \tag{16}$$

Finally, the $1t_{1g}\rightarrow 2t_{2g}$ transition in O_h symmetry corresponds to the spectroscopic transitions

$$^6A_{1g}\rightarrow {}^6A_{1g},\ {}^6E_g,\ {}^6T_{1g},\ {}^6T_{2g} \tag{17}$$

which split in C_{3v} symmetry to give

$$^6A_1\rightarrow {}^6A_1,\ {}^6E,\ {}^6A_2,\ {}^6E,\ {}^6A_1,\ {}^6E \tag{18}$$

Now, as noted previously, the $1t_{2u}$, $6t_{1u}$ and $1t_{1g}$ orbitals of the octahedral cluster mix with each other under the trigonal distortion. Consequently, the states in (14), (16) and (18) with the same symmetry also mix with each other. This being the case, all that can be said precisely is that the average energy of all of the states in (14), (16) and (18) with a given symmetry is given by the average energy of all of the one-electron oribtal transitions which give excited state configurations with that symmetry. For example, in the one-electron orbital description of the trigonally-distorted $(FeO_6)^{9-}$ cluster calculated here, the $2a_2\rightarrow 9a_1$ LMCT type transition, which gives an excited state configuration with $^6A_2$ symmetry, has an energy of only 3.5 eV. This does not imply that there is a spectroscopic $^6A_1\rightarrow {}^6A_2$ transition with that energy, however, it only implies that there is a Slater determinant with that energy. The true $^6A_2$ LMCT states are made up of linear combinations of several Slater determinants with $^6A_2$ symmetry.

The decreased separation between the Fe(3*d*) and O(2*p*) orbitals in the trigonal $(FeO_6)^{9-}$ cluster, therefore, does not have any immediate physical significance. Other clusters with low symmetry such as $(FeO_4(OH)_2)^{7-}$ and $(Fe_2O_{10})^{14-}$ (Sherman 1984a) also show a decreased separation between the O(2*p*) and Fe(3*d*) orbitals. The reason for this is that we are able to separate more of the Slater determinents from each other by removing the orbital degeneracies.

Comparison With Experimental Spectra

The optical spectra of Fe^{3+} systems have been poorly understood. Often, the different ligand field states shown in Figure 7 are obscured by the higher energy LMCT transitions. An additional source of complexity in the spectra of iron (III) oxides and silicates, however, is the effect of magnetic coupling between next nearest neighbor Fe^{3+} cations on the Fe(3*d*) intraconfigurational or ligand field transitions. All of the transitions from the $^6A_1$ ground state to the excited ligand field states involve a two-fold change in spin-multiplicity. As such, all of these transitions are spin-forbidden and one would expect their intensities to be very small. In the spectra of iron oxides and a number of other minerals, however, the nominally spin-forbidden Fe^{3+} ligand field transitions are found instead to be quite intense. The apparent relaxation of the spin selection rule results from the magnetic coupling of next-nearest-neighbor Fe^{3+} cations in the crystal structure (Ferguson et al. 1966; Krebs and Maisch 1971; Lohr 1972; Rossman 1975). If the Fe^{3+} cations in a mineral are magnetically coupled, localized excitations involving a change in spin-multiplicity can occur provided that the net spin of the coupled iron atoms is unchanged. Strong coupling between Fe^{3+} cations in a solid or polynuclear complex will intensify the Fe^{3+} ligand field transitions. This, in turn, will make it difficult to distinguish bands due to these transitions from those due to ligand to metal charge-transfer transitions. Assignments of features to LMCT transitions based on their intensities should be viewed with caution.

To complicate matters further, magnetic coupling between Fe^{3+} cations allows for a new type of electronic transition, namely, the simultaneous excitation of two Fe^{3+} centers by a single photon. These excitations occur at energies given approximately by the sum of two simple Fe^{3+} ligand field transitions. Such transitions have been invoked by Ferguson and Fielding (1972) to account for several features in the spectra of Fe^{3+} in Al_2O_3.

Tables 5 and 6 give spectral band energies for Fe^{3+} cations in both octahedral and tetrahedral coordination in several oxides and silicates. Spectra of the iron oxide and oxide hydroxide polymorphs, particularly in the near-UV, are few. For comparison with the theoretical results described here, however, the most useful experimental data are spectra of dilute Fe^{3+} cations in oxide host phases. In these systems, spectral bands resulting from $Fe^{3+}-Fe^{3+}$ pair interactions can be more easily identified.

Spectra of Octahedral Fe^{3+}

The most extensively investigated system is Fe^{3+} in Al_2O_3 (Krebs and Maisch 1971; Ferguson and Fielding 1972; Lehman and Harder 1970; Tippins 1970). These data are perhaps the most reliable of any Fe^{3+} system studied. Spectra of Fe^{3+} in MgO have been investigated by Blazey (1977); these results are fairly consistent with those for Fe^{3+} in Al_2O_3. The band assignments given here for these systems (Table 5) are in agreement with those of the different investigators.

In addition to the spectra of dilute Fe^{3+} cations in oxide host phases, spectra of two condensed Fe^{3+} phases (hematite and nontronite) are available. The band assignments proposed here for Fe^{3+} in nontronite are somewhat different from those of Karickhoff and Bailey (1973); they did not take spectra in the near-infrared and, hence, did not find the $^4T_1(^4G)$ and $^4T_2(^4G)$ bands at 10.6 and 16.1 kK (Singer 1982). A feature at 19.2 kK was assigned by them to the $^4T_2(^4G)$ band; this feature more likely corresponds to the $^4T_1(^4G)+{}^4T_1(^4G)$ pair excitation.

In their investigation of the optical spectrum of hematite, Marusak et al. (1980) used the calculated one-electron orbital transition energies obtained by Tossell et al. (1973; 1974) to assign spectroscopic features to either "spin-flip" or LMCT transitions. Some of the spectral band assignments given by Marusak et al. (1980), and Tossell et al.

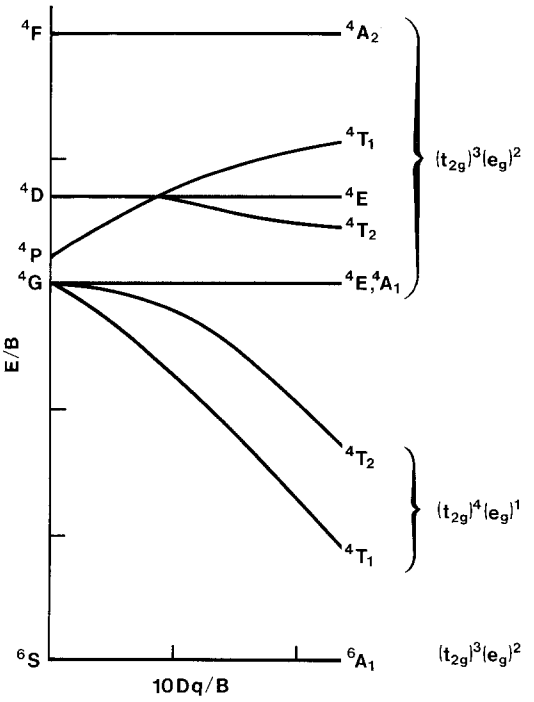

Fig. 7. Tanabe-Sugano diagram for the crystal- or ligand-field states of octahedrally- and tetrahedrally-coordinated Fe^{3+}

Table 5. Observed electronic transition energies in octahedral Fe^{3+} coordination sites in oxides and silicates (in kK)

State	Fe^{3+}: Al_2O_3	Fe^{3+}: MgO	α Fe_2O_3	Nontronite
$^4T_1(^4G)$	9.45	10.0	11.6	10.6
$^4T_2(^4G)$	14.35	13.5	–	16.1
$^4E, {}^4A_1(^4G)$	22.27	21.74	23.8	22.5
$^4T_2(^4D)$	25.51	25.12	–	26.0
$^4E(^4D)$	26.8	27.5	26.7	27.2
$^4T_1(^4P)$	32.5	30.97	31.8	–
$^4A_2(^4F)$	–	–	–	–
$6t_{1u}^{\beta} \rightarrow 2t_{2g}^{\beta}$	38.6	35.8	38.9	38.2
$1t_{2u}^{\beta} \rightarrow 2t_{2g}^{\beta}$	–	40.5	44.8 (?)	–
$6t_{1u}^{\beta} \rightarrow 4e_g^{\beta}$	51.5	46.2	–	50.0
10Dq	15.27	13.4	15.9	14.2
B	0.65	0.48	0.41	0.67
C	3.16	3.38	3.93	3.12
Reference	1–4	5, 6	7	8

1. Krebs and Maisch (1971); 2. Ferguson and Fielding (1971); 3. Lehmann and Harder (1971) 4. Tippins (1970); 5. Blazey (1977); 6. Cheng and Kemp (1971); 7. Marusak et al. (1980); 8. Karickhoff and Bailey (1973)

Table 6. Observed electronic transition energies in tetrahedral Fe^{3+} coordination sites in oxides and silicates (in kK)

State	Fe^{3+}: $LiAlO_2$	Fe^{3+}: SiO_2	Ortho-clase	Phlog-opite
$^4T_1(^4G)$	14.5, 16.3	–	–	–
$^4T_2(^4G)$	18.5, 19.6	18.7, 20.2	20.7	19.0, 20.5
$^4E, ^4A_1(^4G)$	21.6	22.5	22.7	22.6
$^4T_2(^4D)$	22.3	24.8	24.8	24.4
$^4E(^4D)$	25.6	27.3	26.5	26.3
$^4T_1(^4P)$	–	–	–	–
$^4A_2(^4F)$	–	–	–	–
LMCT	–	40.7	–	–
LMCT	–	51.1	–	47.2
$10Dq$	8.35			
B	0.57	0.69	0.55	0.53
C	3.18	3.13	3.43	3.46
Reference	1	2	3	4

1. Waychunas and Rossman (1983); 2. Lehmann (1970); 3. Manning (1970); 4. Karickhoff and Bailey (1973)

(1973) were incorrect; the calculated energies for the one-electron LMCT transitions were too low by about 1.5–2.0 eV (this work) which led to features due to ligand field transitions being misassigned to LMCT transitions. Moreover, the spectra were interpreted by assigning specific one-electron orbital transitions to spectroscopic absorption features. Actually, for the LMCT transitions this may not be a bad approximation (as discussed previously); in general, however, it is physically incorrect.

From the octahedral $(FeO_6)^{9-}$ cluster calculation, the average energy of the $^6A_1(^6S) \rightarrow {}^4T_1(^4G)$ and $^6A_1(^6S) \rightarrow {}^4T_2(^4G)$ transitions is estimated to be 11.13 kK. This compares favorably with the data for $Fe^{3+}:Al_2O_3$ and Fe^{3+}:MgO where the average is about 11.9 kK. For other octahedral Fe^{3+} systems, however, the average energy of these two transitions is somewhat higher; in hematite it is 14 kK while in nontronite it is 13.4 kK.

The average energy of the quartet states arising from the $(2t_{2g})^3(4e_g)^2$ configuration was calculated to be 30.4 kK. This cannot be directly measured experimentally because the high-energy $^4T_1(^4P)$ and $^4A_2(^4F)$ transitions are obscured by the LMCT bands. Still we can estimate an experimental value for the average energy of the quartet states by using the Racah B and C parameters derived from the spectra and the approximate Tanabe-Sugano expression for the average energy (Eq. 13). This gives 28.1 kK for $Fe^{3+}:Al_2O_3$, 27.9 kK for Fe^{3+}:MgO, 28.0 kK for Fe^{3+} in nontronite and 27.8 kK for hematite. Considering the approximations involved, these values are in good agreement with the theoretical MO results.

The value for $10Dq$ in the octahedral $(FeO_6)^{9-}$ cluster is calculated to be 15.8 kK. The Racah B parameter is estimated to be on the order of 640–730 cm^{-1} assuming $C/B = 4.7$. The value for $10Dq$ is in good agreement with those estimated for the systems in Table 5. It is also in good agreement with values obtained from the spectra of goethite (α FeOOH) and lepidocrocite (γ FeOOH) (Mao and Bell 1974). Close agreement between theory and experiments is expected in this case given that previous calculations (Sherman 1984b) on the isoelectronic $(MnO_6)^{10-}$ and comparably covalent $(MnO_6)^{9-}$ clusters also gave accurate values for $10Dq$. The crude estimation of the Racah B parameter value is consistent with the experimental estimates. It should be pointed out that, in ligand field theory, the parameters $10Dq$, B and C are derived assuming that their values are independent of the electronic configuration. In effect, the assumption is made that the $2t_{2g}$ and $4e_g$ orbitals do not relax during electronic transitions. Since this is not the case, the experimental values for $10Dq$, B and C really represent the average values over all the possible electronic configurations. In the approach used here, the values for $10Dq$ and B are derived from the $2t_{2g}$ and $4e_g$ orbital energies in a single configuration. The good agreement between the SCF-Xα-SW results for these parameters and the experimental values, therefore, indicate that ligand field theory provides a good approximation for the spectra of Fe^{3+} oxides and silicates.

The lowest energy LMCT transition, $6t_{1u}{}^{\beta} \rightarrow 2t_{2g}{}^{\beta}$, is calculated to occur at 38.1 kK. This corresponds nearly exactly with the position of a strong band in the spectra of $Fe^{3+}:Al_2O_3$, nontronite, and hematite that has also been assigned by the original investigators of these spectra to a LMCT transition. In Fe^{3+}:MgO, this feature is found at a somewhat lower energy, 35.8 kK, which may reflect a larger $Fe^{3+}-O$ distance. The agreement between the theoretical energy of this one electron orbital transition and the experimental value of the lowest LMCT transition band energy supports the argument given in the previous section, namely, that the spread in energy of the multiplets arising from the $6t_{1u}{}^{\beta} \rightarrow 2t_{2g}{}^{\beta}$ transition ($^6A_{2u}$, ^6E_u, $^6T_{1u}$ and $^6T_{2u}$) is small enough not to perturb their energies.

The next LMCT transition, $1t_{2u}{}^{\beta} \rightarrow 2t_{2g}{}^{\beta}$, corresponds to a set of transitions $^6A_{1g} \rightarrow {}^6A_{1u}$, ^6E_u, $^6T_{1u}$, $^6T_{2u}$ which are calculated to have an average energy of 43.6 kK. Although the $^6A_{1u} \rightarrow {}^6T_{1u}$ transition is Laporte-allowed, it apparently has a fairly low intensity since no feature is resolved at the energy in the spectra of $Fe^{3+}:Al_2O_3$ and nontronite. This band may be obscured by the presumably more intense $^6A_{1g} \rightarrow {}^6T_{1u}$ transition that arises from the $6t_{1u}{}^{\beta} \rightarrow 2t_{2g}{}^{\beta}$ one-electron orbital transition. A feature at 44.8 kK in the spectrum of hematite may correspond to the $1t_{2u}{}^{\beta} \rightarrow 2t_{2g}{}^{\beta}$ set or it may simply be an instrumental artifact resulting from the cutoff of the UV detector.

The next higher energy LMCT transitions are the $^6A_{1g} \rightarrow {}^6T_{1u}$, $^6T_{2u}$ that arise from the $6t_{1u}{}^{\beta} \rightarrow 4e_g{}^{\beta}$ one-electron orbital transition. The energy of the latter is calculated to be 51.9 kK. This energy corresponds to that of a feature at 51.5 and 50.0 kK in the spectra of $Fe^{3+}:Al_2O_3$ and nontronite, respectively, and may also correspond to the band at 46.1 kK in the spectra of Fe^{3+}:MgO. In the spectra of these systems, this band is considerably more intense than that associated with the $6t_{1u}{}^{\beta} \rightarrow 2t_{2g}{}^{\beta}$ transition. This may be explained, in part, by noting that the $6t_{1u}{}^{\beta} \rightarrow 2t_{2g}{}^{\beta}$ transition corresponds to four spectroscopic transitions $^6A_{1g} \rightarrow {}^6A_{2u}$, ^6E_u, $^6T_{1u}$, $^6T_{2u}$ with only the $^6A_{1g} \rightarrow {}^6T_{1u}$ allowed while the $6t_{1u}{}^{\beta} \rightarrow 4e_g{}^{\beta}$ transition corresponds to only two spectroscopic transitions $^6A_{1g} \rightarrow {}^6T_{1u}$, $^6T_{2u}$ with the $^6A_{1g} \rightarrow {}^6T_{1u}$ transition being allowed. As such, we can observe one-half of the transitions associated with the $6t_{1u}{}^{\beta} \rightarrow 4e_g{}^{\beta}$ transition but only one-fourth of the transitions associated with the $6t_{1u}{}^{\beta} \rightarrow 2t_{2g}{}^{\beta}$ transition.

Spectra of Tetrahedral Fe^{3+}

The spectrum of tetrahedrally coordinated Fe^{3+} in $LiAlO_2$ (Waychunas and Rossman 1983) is of particular interest

Table 7. Number of electrons donated to Fe atoms by each type of orbital interaction

	$(FeO_6)^{9-}$ O_h			$(FeO_6)^{9-}$ C_{3v}			$(FeO_4)^{5-}$ T_d	
	α spin	β spin		α spin	β spin		α spin	β spin
e_g (σ)	−0.009	−0.474						
t_{2g} (π)	−0.365	−0.273				e	−0.173	−0.276
t_{1u}	−0.191	−0.150	e	−0.374	−0.763	t_2	−0.182	−0.837
a_{1g} (σ)	−0.128	−0.106	a_1	−0.292	−0.280	a_1	−0.134	−0.114
Total	−0.693	−1.003		−0.666	−1.043		−0.489	−1.227
Net charge on Fe	+1.304			+1.291			+1.284	
Net spin on Fe	4.69 μ_B			4.623 μ_B			4.260 μ_B	

since the mean Fe−O bond length in this system was determined by EXAFS to be 1.82 A. This is fairly similar to the bond distance in the $(FeO_4)^{5-}$ cluster calculation presented here (1.865 Å). Waychunas and Rossman (1983) did not assign the absorption bands in the optical spectra; proposed band assignments are given in Table 6. Lehmann (1970), obtained the spectrum of Fe^{3+} in the tetrahedral interstitial site of low-quartz (α SiO_2) and assigned features at 18.7 and 20.2 kK to the $^6A_1 \rightarrow {}^4T_1({}^4G)$ and $^4T_2({}^4G)$ transitions, respectively. Likewise, Karickhoff and Bailey (1973) assigned the 19.0 and 20.5 kK features in the spectra of tetrahedral Fe^{3+} in phlogopite to these transitions. The band assignments given here differ in that these two features are assigned to split components of the $^4T_2({}^4G)$ state. Both the $^4T_1({}^4G)$ and $^4T_2({}^4G)$ states are usually split by the dynamic Jahn-Teller effect. The revised assignment scheme presented here is in closer agreement with the data of Waychunas and Rossman (1983) and, as will be shown below, with the $(FeO_4)^{5-}$ cluster calculation.

The average energy of the $^4T_1$ (^4G) and $^4T_2({}^4G)$ transitions of the tetrahedral $(FeO_4)^{5-}$ cluster was calculated to be 16.2 kK. This argues against the assignments given by Lehmann (1970) and Karickhoff and Bailey (1973) for the $^4T_1({}^4G)$ and $^4T_2({}^4G)$ bands. The calculated average energy is in reasonable agreement with the data for Fe^{3+}:$LiAlO_2$ if the band assignment given in Table 6 is used.

The average energy of the quartet states arising from the $(2e)^2(6t_2)^3$ configuration was calculated to be 25.9 kK. Using the band assignments and the resulting values for B and C, the experimental average energy is estimated to be 26.7 kK for Fe^{3+}:$LiAlO_2$, 27.8 for Fe^{3+} in orthoclase, 28.1 kK for Fe^{3+}:SiO_2, and 27.6 kK for Fe^{3+} in phlogopite. The agreement between theory and experiment is fairly good for Fe^{3+}:$LiAlO_2$ where the Fe−O bond lengths are known to be similar to those of the $(FeO_4)^{5-}$ cluster. As will be discussed below, the $(FeO_4)^{5-}$ cluster calculation indicates that the effective spin on the Fe atom is smaller in the $(FeO_4)^{5-}$ cluster than in the $(FeO_6)^{9-}$ cluster. A smaller effective spin results in a decreased exchange splitting of the Fe(3d) orbitals in the $(FeO_4)^{5-}$ cluster. In accordance with the decreased exchange splittings, the average energy of the quartet states in the $(FeO_4)^{5-}$ cluster should also be smaller, as was calculated. The experimental data indicate that this picture is qualitatively correct but, on the other hand, the calculations seem to exaggerate the magnitude of the effect.

The value for $10Dq$ in $(FeO_4)^{5-}$ was estimated to be 8.23 kK using the approach of Sambe and Felton (1976). If the energy of the $^4T_1({}^4G)$ state is taken to be the average energy of the 14.5 and 16.3 kK bands, then the experimental value for $10Dq$ is estimated to be 8.35 kK. This value also predicts the $^4T_2({}^4G)$ band energy with the expected accuracy. The close agreement between the SCF-Xα-SW and experimental values for $10Dq$ lends further support for the band assignments given in Table 6.

The lowest energy LMCT transition of the $(FeO_4)^{5-}$ cluster is the $1t_1^{\beta} \rightarrow 2e^{\beta}$ which was calculated to have an energy of 40.4 kK. This agrees well with the spectrum of Fe^{3+}:SiO_2 where the first LMCT band is observed at 40.7 kK. No feature near 40 kK is found in the spectrum of Fe^{3+} in phlogopite but a broad shoulder at 35.7 kK in one sample was observed by Karickhoff and Bailey (1973). This feature was assigned by Faye (1968) to $Fe^{3+} \rightarrow Al^{3+}$ charge-transfer. More likely, it corresponds to the $1t_1^{\beta} \rightarrow 2e^{\beta}$ LMCT transition. Bands observed at 51.5 kK and 47.2 kK in the spectra of Fe^{3+}:SiO_2 and Fe^{3+} in phlogopite, respectively, can be readily assigned to the $1t_1^{\beta} \rightarrow 6t_2^{\beta}$ transition.

The lowest energy LMCT transitions of octahedrally- and tetrahedrally-coordinated Fe^{3+} occur well into the near-ultraviolet. Although the tails of these transitions contribute to some of the absorption by Fe^{3+} in the visible region, they are not responsible for the visible region absorption edge observed in the spectra of Fe^{3+} oxides and silicates. Spectra of isolated Fe^{3+} centers in solids or mononuclear complexes show only weak absorbance in the visible region (e.g. Lehmann 1970; Rossman 1975); indeed, such systems are nearly colorless. In systems where Fe^{3+} centers are magnetically coupled with each other, however, the characteristic visible region absorption edge is present. Hence, most of the visible region absorption in iron oxides and silicates is due to ligand field transitions which have been intensified by the Fe−O−Fe superexchange interaction. The pair excitations, not addressed here, may also contribute to the visible region absorption edge.

Applications to the Physical Properties and Crystal Chemistry of Iron Oxides

Ionic vs. Covalent Bonding

The Fe−O chemical bond is partially covalent so that electronic charge is donated to the Fe^{3+} center by the O^{2-} anion coordination environment. Covalency, however, is not a quantum mechanical observable and, as such, it is

not possible to give a quantitative measure of covalency without invoking an arbitrary scheme for partitioning the electronic charge among the atoms. The results of the SCF-Xα-SW calculations give the electronic charge within each of the atomic spheres and within the interatomic region. One approach to partitioning the electronic charge among the atoms is to partition the interatomic charge of a given orbital according to the ratio of the atomic charges of the orbital. The results of this procedure are given in Table 7 which shows the net electronic charge (number of electrons) of each spin donated to the different Fe^{3+} centers by each type of orbital interaction. The results show that, in each cluster, the Fe−O bond is about 56% covalent; the charge on the Fe atom is reduced from +3 to about +1.3. Note that the covalency of the Fe−O bond is essentially the same in the octahedral, tetrahedral, and trigonally-distorted octahedral clusters. On the other hand, the nature of the Fe−O covalency, in particular its spin-polarization, differs appreciably among the clusters. The effect of covalency on the spin-population (and effective magnetic moment) at the Fe^{3+} site can be related to the magnetic structures of Fe^{3+} oxides; this will be discussed below.

The bonding in the trigonally distorted $(FeO_6)^{9-}$ cluster is interesting insofar as there are two different oxygen sites. The Fe−O(2) bond is somewhat more covalent than the Fe−O(1) bond. This is contrary to what one might expect given that the Fe−O(2) bond length (2.117 Å) is considerably greater than the Fe−O(1) bond length (1.950 Å). Apparently, the strong repulsive interactions across the short (2.669 Å) O(2)−O(2) bonds promote the Fe−O(2) bonding interaction. (One might argue that the covalency of the Fe−O(2) bond is greater than that of the Fe−O(1) bond because the atomic sphere radius of the O(2) atom is greater than that of the O(1) atom. This does not appear to be the case since the atomic sphere overlap of the Fe−O(2) bond is much smaller than that of the Fe−O(1) bond.)

Magnetism in Iron Oxides

An important aspect of the Fe−O chemical bond is its spin polarization. In the $(FeO_6)^{9-}$ cluster, the α-spin e_g and t_{2g} antibonding orbitals are occupied and cancel much of the α-spin t_{2g} and e_g Fe−O bonding interaction. At the same time, the β-spin antibonding orbitals are unoccupied. Consequently, most of the net electronic charge donated to the Fe^{3+} center by the O^{2-} anions is of β-spin character (see Table 7). The spin-dependent covalency leaves the oxygen atoms with a net α-spin excess. The oxygen atoms will therefore favor donating α-spin electronic charge to any other Fe^{3+} centers to which they are bonded. This can be done only if the antibonding orbitals localized on these Fe^{3+} centers are occupied by β-spin electrons; that is, if these Fe^{3+} centers are antiferromagnetically coupled to the first Fe^{3+} center. It follows, therefore, that the spin-polarized calculations on simple $(FeO_6)^{9-}$ clusters predict the occurrence of the antiferromagnetic superexchange interaction observed in Fe^{3+} oxides and silicates. The same result follows from the nature of the bonding in the $(FeO_4)^{5-}$ cluster.

We can apply this idea to the magnetic structures of iron oxides. In spinel-structure oxides such as magnetite or maghemite, Fe atoms in the octahedral *B* sites are coupled antiferromagnetically with Fe atoms in the tetrahedral *A* sites. This forces the *B* site cations to be ferromagnetically coupled to each other. This magnetic structure implies that the *A*–*B* site antiferromagnetic coupling is stronger than the *B*–*B* site antiferromagnetic coupling. The results given in Table 7 show that the net electronic spin at the tetrahedral Fe^{3+} center is much smaller than that at an octahedral Fe^{3+} center. Hence, the electronic spin of an O^{2-} anion is polarized more strongly by the *A*-site Fe^{3+} center than by the *B*-site Fe^{3+} center. This, in turn, results in the Fe(*A*)−O−Fe(*B*) antiferromagnetic interaction being stronger than the Fe(*B*)−O−Fe(*B*) antiferromagnetic interaction.

The magnetic structure of hematite is such that the Fe^{3+} ions are antiferromagnetically coupled across the shared faces along the *c* axis but ferromagnetically coupled within the basal planes perpendicular to the *c* axis. Within the basal planes, FeO_6 polyhedra share edges and corners. This magnetic structure follows if the antiferromagnetic interaction between face-sharing FeO_6 polyhedra is stronger than that between edge- and corner-sharing FeO_6 polyhedra. In the context of the simple FeO_6 and FeO_4 clusters, one might expect the face-sharing antiferromagnetic interaction to be stronger than the edge-or corner-sharing antiferromagnetic interaction simply because face-sharing FeO_6 polyhedra have three ligands in common while edge- or corner-sharing FeO_6 polyhedra have only two, or one, ligands in common. In addition to the greater number of shared ligands associated with the face-sharing octahedra arrangement, strong antiferromagnetic coupling between face-sharing octahedra is promoted by the trigonal distortion of the Fe^{3+} coordination site. In the trigonally-distorted $(FeO_6)^{9-}$ cluster, the Fe^{3+} center induces a greater α-spin population on the O(2) oxygens than on the O(1) oxygens. Hence, the Fe−O(2)−Fe antiferromagnetic interaction will be stronger than the Fe−O(1)−Fe antiferromagnetic interaction. Since the O(2) oxygens are those which bridge the face-sharing FeO_6 polyhedra, it follows that the face-sharing FeO_6 sites will be antiferromagnetically coupled to each other but edge-sharing coordination sites will be ferromagnetically coupled. Note, therefore, that we need not invoke any metal-metal bonding interaction across the shared faces to account for the magnetic structure of hematite.

The calculated effect of chemical bonding on the spin populations at the different atoms can be addressed by results of polarized neutron diffraction studies (Tofield 1975; 1976) and magnetic hyperfine measurements on Fe^{3+} coordination sites in oxides. The cluster calculations presented here estimate the magnetic moments of Fe^{3+} in octahedral and tetrahedral sites in oxides to be 4.69 and 4.26 μ_B, respectively. These are very close to values obtained experimentally: In ferrites, the octahedral Fe^{3+} and tetrahedral Fe^{3+} moments are 4.62 and 4.31 μ_B (Sawatzky and van der Woude 1974). The *B*-site Fe^{3+} moment in magnetite is estimated to be 4.55 μ_B (Dickof et al. 1980). In short, the Fe−O covalency reduces the Fe^{3+} magnetic moment from its free ion value of 5 μ_B. The smaller moment of tetrahedrally-coordinated Fe^{3+} is due to a greater spin dependent covalency. Previous $(FeO_6)^{9-}$ and $(FeO_4)^{5-}$ cluster molecular orbital calculations, using the Discrete Variational method (Xα exchange but with the LCAO approximation) have been done by Byrom et al. (1975) These results also showed that, because of covalency, the magnetic moment of tetrahedrally-coordinated Fe^{3+} is smaller than that for octahedrally-coordinated Fe^{3+}.

Several aspects of the Fe–O bond that are given in Table 7 can be related to the Mössbauer spectra of iron oxides First, the isomer shifts (relative to metallic iron) of tetrahedrally coordinated Fe^{3+} are generally smaller than those of octahedrally coordinated Fe^{3+}. In γ Fe_2O_3, for example, the isomer shift of tetrahedral Fe^{3+} is 0.27 mm/sec while that for octahedral Fe^{3+} is 0.41 mm/sec (Goodman 1982). The isomer shift (relative to metallic iron) will decrease with increasing *s*-electron charge density at the Fe nucleus. From Table 7 we find that the net 4*s* orbital population is greater in the $(FeO_4)^{5-}$ cluster than in the $(FeO_6)^{9-}$ cluster and, accordingly, the *s*-electron charge density at the nucleus is probably greater in $(FeO_4)^{5-}$ than in $(FeO_6)^{9-}$. Tang Kai et al. (1980) have shown that with decreasing Fe–O distance, the isomer shift in $(FeO_4)^{5-}$ decreases, due to increased Fe–O covalency. This may also explain the decreased isomer shift of tetrahedrally coordinated Fe^{3+} relative to that of octahedrally coordinated Fe^{3+}.

The effective magnetic field at the Fe nucleus is generally smaller in tetrahedrally-coordinated Fe^{3+} than in octahedrally-coordinated Fe^{3+} (e.g. Gibb 1976). The magnetic field at the Fe^{3+} nucleus arises only from the Fermi contact interaction and, as such, should be dependent upon the net effective spin at the Fe site. In agreement with the trend observed in the Mössbauer spectra, the net α-spin density at the Fe site in the $(FeO_4)^{5-}$ cluster is calculated to be smaller than that in the $(FeO_6)^{9-}$ clusters. Note, however, that the calculations probably exaggerate the difference in spin densities.

Comparison with other Calculations

The major differences between the $(FeO_6)^{9-}$ and $(FeO_4)^{5-}$ results (using overlapping atomic spheres) presented here and the earlier results (using tangent atomic spheres) of Tossell et al. (1973) and Tossell (1978) concern the exchange splittings of the Fe 3*d* type orbitals, the O 2*p*–Fe 3*d* energy separation and the value of the crystal field splitting. The qualitative picture of the electronic structure of iron oxides is the same in both calculations. In the multiple-scattering method, the potential in the interatomic region is constant. Accordingly, the wave functions in this region are delocalized partial waves. If tangent, rather than overlapping, atomic spheres are used the interatomic volume is increased which, in turn, tends to overdelocalize the molecular orbital wavefunctions. The effect of this delocalization is to decrease the exchange splittings of the orbitals and, hence, decrease the energy of the β-spin Fe 3*d* type orbitals relative to that of the O 2*p* valence band orbitals. Hence, the more reasonable exchange splittings of the Fe 3*d* type orbitals and the improved values of the LMCT energies in the overlapping sphere calculations are a consequence of decreasing the volume of the physically undesireable intersphere region.

Conclusions

The Fe–O chemical bond in Fe^{3+} oxides is found to be fairly covalent. This agrees with the observed Lewis acidity of Fe^{3+} in aqueous systems and also provides a qualitative explanation for the structural diversity of iron oxides. The spin unrestricted calculations show how the phenomenon of superexchange leading to antiferromagnetism can be easily understood in terms of the nature of the Fe–O chemical bond.

Calculated energies of transitions observed in the optical spectra of Fe^{3+} oxides and silicates are in good agreement with experimental results. The lowest energy ligand to metal charge transfer transition energies for FeO_6 coordination polyhedra are calculated to be about 4.7 eV (38 kK). This is in agreement with spectroscopic data on a wide variety of octahedral Fe^{3+}-oxo complexes and minerals. Moreover, this particular result implies that most of the strong optical absorption in the visible and near-ultraviolet spectra of Fe^{3+} oxides and silicates is due to Fe^{3+} ligand field transitions which have been intensified by Fe^{3+}–Fe^{3+} pair interactions. Using multiplet theory, the diagonal sum rule, and the Tanabe-Sugano expressions of ligand field theory, values of $10Dq$ and B were calculated from the one-electronorbital energies. The values obtained are in good agreement with those estimated from experimental spectra of iron oxides. An important aspect of the multiplet theory approach is its ability to relate the conceptually useful one-electron orbital picture with experimental spectra. For example, the Racah B and C parameters are shown to be directly proportional to the exchange splittings of the one-electron Fe^{3+} 3*d* type orbitals (the $2t_{2g}$ and $4e_g$). The exchange splittings of these orbitals are, in turn, a direct function of the spin-down *versus* spin-up charge density donated to the Fe^{3+} center by the oxygen ligands. Further calculations on other Fe^{3+} centered clusters and comparison with optical spectra are expected to provide more insight on the relation between chemical bonding and electronic spectra of Fe^{3+} minerals and complexes.

Acknowledgements. Special thanks are due to R.G. Burns and K.H. Johnson for helpful comments and discussions. This work was supported by NSF Grant No. EAR 8313585, awarded to R.G. Burns, to study chemical bonding in iron and manganese oxides.

References

Blake RL, Hessevick RE, Zoltai T, Finger LW (1966) Refinement of the hematite structure. Am Mineral 51:123–129

Blazey KW (1977) Optical absorption of MgO:Fe. J Phys Chem Solids 38:671–675

Byrom E, Freeman AJ, Ellis DE (1975) Covalency effects on tetrahedral and octahedral Fe^{3+} sites in YIG: charge and spin densities and neutron form factors, AIP Conference Proceedings 24, Magnetism and Magnetic Materials 1974:209–210

Cheng JC, Kemp JC (1971) Magneto-optical study of the spin-lattice relaxation of Fe^{3+} in MgO. Phys Rev B4:2841–2846

Dickof PA, Schurer PJ, Morrish AH (1980) Magnetic structure of zinc substituted magnetite at 4.2 K. Phys Rev B22:115–127

Faye GH (1969) The optical absorption spectrum of tetrahedrally coordinated Fe^{3+} in orthoclase. Can Mineral 10:112–117

Fasiska EJ (1967) Structural aspects of the oxides and oxyhydrates of iron. Corros Sci 7:833–839

Ferguson J, Guggenheim HJ, Tanabe Y (1966) The effects of exchange interactions in the spectra of octahedral manganese II compounds. J Phys Soc Jap 21:347–354

Ferguson J, Fielding PE (1972) The origins of the colours of natural yellow, blue and green sapphires. Aust J Chem 25:1371–1385

Gibb TC (1976) Principles of Mossbauer spectroscopy. Chapman and Hill, London

Goodman BA (1982) Mossbauer spectroscopy. In: Fripiat JJ (ed) Advanced techniques for clay mineral analysis. Elsevier, Amsterdam, pp 113–137

Johnson KH (1973) Scattered wave theory of the chemical bond. Adv Quantum Chem 7:143–185
Johnson KH, Smith FC (1972) Chemical bonding of a molecular transition metal ion in a crystalline environment. Phys Rev B1:831–843
Karickhoff SW, Bailey GW (1973) Optical absorption spectra of clay minerals. Clays Clay Miner 21:59–70
Krebs JJ, Maisch WG (1971) Exchange effects in the optical absorption spectra of Fe^{3+} in Al_2O_3. Phys Rev B4:757–769
Lehmann G (1970) Ligand field and charge-transfer spectra in Fe (III)-O Complexes. Z Phys Chem NF 72:279–297
Lehmann G, Harder H (1970) Optical spectra of di- and trivalent iron in corundum. Am Mineral 55:98–105
Lever ABP (1968) Inorganic Electronic Spectroscopy. Elsevier, Amsterdam
Lohr LL (1972) Spin-forbidden electronic excitations in transition metal complexes. Coord Chem Rev 8:241–259
Manning PG (1970) Racah parameters and their relationships to lengths and covalencies of Mn^{2+} and Fe^{3+} oxygen bonds in silicates. Can Mineral 10:677–687
Mao HK, Bell PM (1974) Crystal field effects of ferric iron in goethite and lepidocrocite: Band assignments and geochemical application high pressure. Carnegie Inst Washington, Yearb 1973:502–507
Maruthe VR, Trautwein A (1983) Calculation of charge density, electric field gradient and internal magnetic field at the nuclear site using molecular orbital cluster theory. In: Thosar BV (ed) Advances in Mossbauer Spectroscopy, pp 398–449
Marusak LA, Messier R, White WB (1980) Optical absorption spectrum of hematite, α-Fe_2O_3, near IR to near UV. J Phys Chem Solids 41:981–984
Norman JG (1976) Non-empirical versus empirical choices for overlapping sphere radii ratios in SCF-X α -SW calculations on ClO_4- and SO_2. Mol Phys 31:1191–1198
Rossman GR (1975) Spectroscopic and magnetic studies of ferric iron hydroxy sulphates: intensification of color in ferric iron clusters bridged by a single hydroxide ion. Am Mineral 60:698–704
Salahub DR, Messmer RP, Johnson KH (1976) Ionization potentials and bond lengths for CO, N_2 and F_2 using the SCF-X α- SW: a study of the effect of overlapping spheres. Mol Phys 31:529–534
Sambe H, Felton RH (1976) Connection between the X α method and ligand field theory. Int J Quantum Chem Symp 10:155–158
Sawatzky GA, van der Woude F (1974) Covalency effects in hyperfine interactions. J Phys 35:C6:47–60
Schwarz K (1972) Optimization of the statistical exchange parameter α for the free ions H through Nb. Phys Rev B5:2466–2468
Sherman DM (1984a) The electronic structures of iron and manganese oxides with applications to their mineralogy. Ph D dissertation, Massachusetts Institute of Technology
Sherman DM (1984b) The electronic structures of manganese oxide minerals. Am Mineral 69:788–799
Singer RB (1982) Spectral evidence for the mineralogy of the high albedo soils and dusts on Mars. J Geophys Res 87:10159–10168
Slater JC (1968) Average energy of states of given multiplets in atoms. Phys Rev 165:655–658
Slater JC (1974) The self-consistent field method for atoms, molecules and solids. McGraw-Hill, New York
Tang Kai A, Annersten H, Ericsson T (1980) Molecular orbital (MSX α) calculations of *s*-electron densities of tetrahedrally coordinated ferric iron: comparison with experimental isomer shifts. Phys Chem Minerals 5:343–349
Tippens HH (1970) Charge-transfer spectra of transition metal ions in corundum. Phys Rev B1:126–135
Tofield BC (1976) Covalency effects in magnetic interactions. J Physique (Paris) 37:C6539–C65969
Tofield BC (1975) The study of covalency by magnetic neutron scattering. Struct Bonding (Berlin) 21:1–88
Tossell JA (1980) Electronic structure of dichalcogenide and dipnictide anions. J Phys Chem Solids 41:1047–1052
Tossell JA (1978) Self-consistent-field-X α study to one-electron energy levels in Fe_3O_4. Phys Rev B17:484–487
Tossell JA, Vaughan DJ, Johnson KH (1974) The electronic structure of rutile, wustite and hematite from molecular orbital calculations. Am Mineral 59:319–334
Tossell JA, Vaughan DJ, Johnson KH (1973) Electronic structure of ferric iron octahedrally coordinated to oxygen. Nature Phys Sci 244:42–45
Verdonck E, Vanquikenborne G (1976) Charge transfer spectra of octahedral transition metal complexes. Inorg Chim Acta 23:67–76
Waychunas GA, Rossman GR (1983) Spectroscopic standard for tetrahedrally coordinated ferric iron: $LiAlO_2$:Fe^{3+}. Phys Chem Minerals 9:212–215

Received March 5, 1984